ACS Photonics

Article

pubs.acs.org/journal/apchd5

Nanoscale Charge Separation Using Chiral Molecules

Nir Peer,[†] Irene Dujovne,[†,‡] Shira Yochelis,[†] and Yossi Paltiel[†,*]

[†]Department of Applied Physics, The Hebrew University of Jerusalem, Givat Ram, Jerusalem 9190401, Israel

[‡]Department of Physics, University of Massachusetts, Amherst, Massachusetts 01003, United States

ABSTRACT: Charge separation is a fundamental process currently being used in a large variety of devices. Typically, charge separation requires doped P/N junctions that, at the nanoscale, are difficult to form due to the small number of participating atoms. Thus, it is not trivial to separate charges at the nanometric scale in a simple flexible way. Recently, studies of electron transfer through organic helical chiral molecules have shown that electron transmission through these molecules is spin-dependent at ambient temperatures. Utilizing semiconductor nanocrystals and helical chiral molecules, we created a room-temperature optically activated, thin-layer, charge-separating nanoscale device. Total efficiency of separation is sensitive to the polarization of the light and could be enhanced by chiral imprinting on the NCs. The fabrication process is simple and uses self-assembly methods that could be applied to a wide variety of nanocrystal-based devices. From the fundamental point of view the induced chiral charge separation may be relevant for physical and biological processes such as charge separation in photosynthesis.

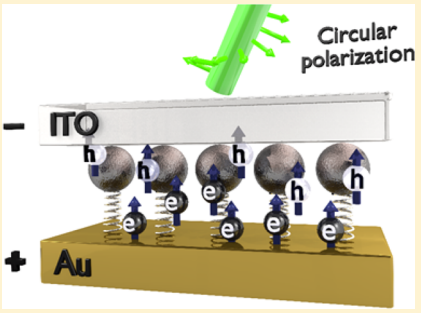

KEYWORDS: *chiral molecules, charge separation, spin, polarization, excitons, CISS*

Charge separation is essential for a large variety of optoelectronic devices, such as solar cells and photodetectors.[1] A subset of these devices are photovoltaic devices, that are charge-separating systems operating by light energy.[2] Nowadays, these systems are mainly based on doped silicon, in which a junction is formed between a donor dopant (p-type) and an acceptor dopant (n-type). Charge diffusion equalizes the Fermi energy of both layers creating an electric field called the "depletion region" that has built-in potential. Under an applied bias voltage and above bandgap illumination, the device will create an electron−hole pair that will be separated according to the built-in potential. One of the main drawbacks in these devices arises when miniaturization is required since the amount of doping in a semiconductor is limited to the maximum concentration of $10^{19}(\text{dopants/cm}^3) = 10^{-2}(\text{dopants/nm}^3)$, over which the material is considered degenerate at room temperature.[3] This means that typically there is less than a single dopant per cubic nanometer, thus, making it almost impossible to create a doping-controlled charge separation at the nanoscale.

In recent years, studies of electron transfer through organic helical chiral molecules have shown that electron transmission through these molecules is spin-dependent at ambient temperatures.[4,5] Particularly, it has been revealed that chiral helical molecules can serve as efficient spin filters due to strong spin orbit coupling mechanisms and different spin transfer probabilities,[6−13] thus, creating a chiral-induced spin selectivity (CISS) effect.

The spin selectivity of charges transported through chiral molecule is dependent on the charge sign, the current direction, and on the handedness of the molecule.[8] Therefore, by controlling the electron−hole spin states in nanostructures, using different circularly polarized light excitation, we affect the probability of the charges with certain spin to be transferred through the chiral monolayer. Similar behavior was observed in the study of local spin-based magnetization via charge transfer in self-assembled monolayer (SAM) of chiral polyalanine molecules.[5]

Semiconductor nanocrystals (NCs), often called quantum dots, are very versatile due to the tunability of their optical and electronic properties by their size, shape, and composition,[14,15] making them ideal for photonic devices. Photoexcitation of a strongly confined NC system, such as CdSe, results in the formation of excitons with known spin states.[16] Previous experiments have shown processes of a fast hole spin-flip in CdSe NCs, which enables the creation of electron−hole pairs with equal sign of spin states $(S_e,S_h)_{\pm1/2,\pm3/2}$.[17−19] The spin direction is then dependent on the circular polarization of the exciting light.[20,21] By using organic molecules, covalent selective adsorption of the CdSe NCs can be achieved.[22] For example, by coupling the NCs to a field effect transistor (FET), our group has previously shown that a room temperature spectrally tunable light detector can be realized.[23] Using chiral linkers covalently bond to the NCs could imprint the chirality on the NCs. An effect originated due to strong spin orbit coupling induced at the NCs surfaces on which helix chiral molecules are adsorbed.[24−26] This effect should induce asymmetry to the NCs spin states even for nonpolarized excitation.

In the present study, we demonstrate nanoscale charge separation in a thin layer device based on helical chiral molecules and semiconductor NCs. We combined a SAM of

Received: June 22, 2015
Published: September 29, 2015

DOI: 10.1021/acsphotonics.5b00343
ACS Photonics 2015, 2, 1476−1481

polyalanine with NCs and measured the induced photocurrent when the NCs are illuminated with light polarized in different ways. By applying circularly polarized light it was possible to generate charge separation in this system. The significant difference in the current responses on the nanometric scale was attributed to the CISS effect and to room temperature charge separation. Similar devices can be simply fabricated in large scale and can be adapted to a wide variety of NCs.

RESULTS

Current response was measured under illumination with different light polarizations: clockwise (CW), counter clockwise (CCW), and linear. The *I*−*V* curves are displayed in Figure 2a.

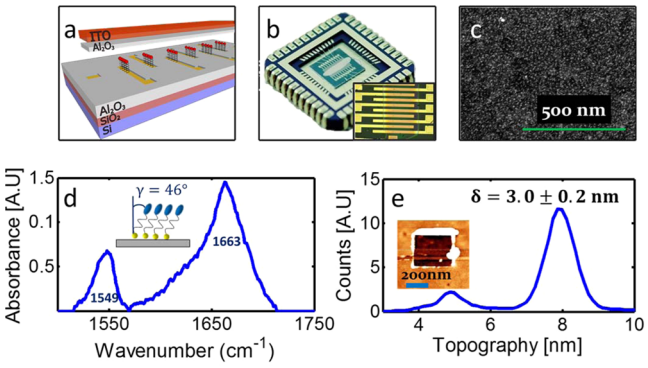

Figure 1. (a) Schematic drawing of the device structure. *I*−*V* measurements are done between the lower gold and upper ITO contacts. (b) Photo of device mounted and wire bonded to a 44 header chip. In the inset is a microscope picture of the active area in the device. (c) SEM image of CdSe NCs with the main emission peak at 610 nm, adsorbed on top of a chiral molecules monolayer on gold. (d) PM-IRRAS spectra of L-polyalanine monolayer on a gold surface. The energies of amide-I and amide-II vibrations indicate that the monolayer is in a helix form. From their ratio the tilt angle of the molecules adsorption relatively to the surface normal can be obtained. (e) Histogram of the topography information on the sample surface where a portion of the chiral monolayer was removed in the middle (inset) measured by AFM. The height difference between the surface and the scratched area implies that the layer thickness is 3 nm.

The dark current (black line) has a diode-like shaped feature resulting from the Au−NCs−ITO interface in the device. The illuminated measurements show a conductance that is light polarization dependent. This response is governed by both coherent spin relaxation processes and fast noncoherent processes.[27] In order to retain solely the polarization dependence for the current response, we subtract the linear polarization response from the CCW and CW circular polarization (Figure 2b). In negative bias, the CW circular polarization response is stronger, while in forward bias, the CCW polarization has a stronger response. In both cases, the holes and electrons are separated but with different efficiencies. Since linear polarization carries both CW and CCW circular polarization probabilities equally, smaller charge separation effect should be observed. Chiral imprinting on the NCs by the organic linkers will enhance the response of one circular polarization.

By selectively controlling the electron−hole spin states with different circularly polarized light, we affect the probability of the charges transfer through the chiral monolayer. CW and CCW circular polarized light creates electrons with favored or unfavored spin states according to the CISS effect where the

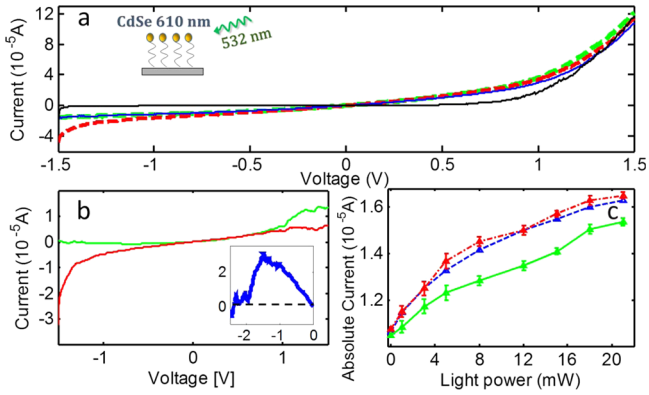

Figure 2. (a) *I*−*V* curve of a device with adsorbed CdSe NCs (610 nm main emission peak) on top of helical chiral molecules, under polarized light illumination. The *I*−*V* curves for the three illumination polarizations (red, CW; blue, linear; green, CCW) show distinct current responses stronger than the dark current (black). (b) CCW (green) and CW (red) polarization current responses after the linear current was subtracted from them. The CW polarization creates electrons with favored spins, which are driven with less resistance through the chiral molecules for reversed voltage bias. On the other hand, the holes do not have the required spin state; therefore, in forward bias, the CCW polarization has a stronger response. In the inset, the response difference between CCW and CW circular polarizations with bias extended to −2.5 V is plotted. The current difference between polarizations diminishes when the bias voltage reaches about 2 V, possibly due to the CISS pseudogap. (c) Absolute current response as a function of excitation power for different light polarizations (red, CW; blue, linear; green, CCW) under a constant bias of −1.5 V.

charge transfer probability is dependent on the charge sign as well as on the favored spin state.[28] These electrons are driven through the chiral molecules once a negative voltage bias is applied. For a given bias voltage on the device, we expect higher current for a selected circular polarization than the counter circular polarization. Furthermore, this trend is expected to flip once the bias voltage is reversed, giving rise to antisymmetric *I*−*V* curves for negative and positive biases. For our chiral SAM, CW polarized light creates electrons with favored spin states, while the holes do not have the required spin state to be transferred through the chiral molecules; therefore, charge separation is created. This effect is schematically portrayed in Figure 4a where the device is under illumination of CW circular polarized light, and a negative bias is applied. The light creates electron−hole pairs with spin facing up, and the bias drives the electrons downward through the chiral molecules. The spin and charge values of these electrons are favored by the CISS effect, therefore the current will be higher than electrons with spin down (CCW polarization) or holes with spin up (positive bias). In a general energetic perspective, a model is suggested in Figure 4b, with a pseudo CISS gap that changes according to the polarization on the device. Charges carrying the favored spin will have energetic preference to transfer through the chiral monolayer. The efficiency of the effect is influenced by four lifetimes. The decay lifetime of the excited NCs to the preferable exciton spin state. This time is controlled by the NCs size and type, the NCs surface and the temperature. Usually this time is very fast.[17−19] The other competing times are the electron drift time to the contacts and T1 of the chiral gold substrate or the NCs. Charge separation should occur before the spin state decay.

DOI: 10.1021/acsphotonics.5b00343
ACS Photonics 2015, 2, 1476−1481

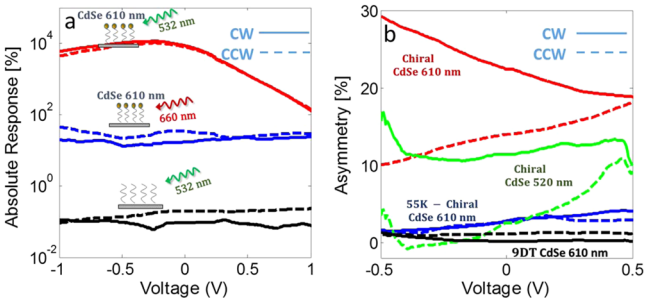

Figure 3. (a) Absolute response of three different setups, comparing the CW (solid) and CCW (dashed) response to dark current response and giving information whether the devices react to the illuminations. As seen, the device with chiral molecules and NCs (red curves) illuminated above bandgap has a response 2 orders of magnitude larger than a device with below band gap illumination (blue curves) and 4 orders of magnitude larger than a device without NCs (black curves). (b) Asymmetry between the circular polarization normalized to the linear response, for four different devices. For the device with chiral molecules and 610 nm CdSe NCs (red curves) a distinct asymmetry is seen between CW and CCW illuminations, especially in the negative bias, thus showing long spin coherence times, enabling a more efficient charge separation. This asymmetry is slightly smaller for smaller NCs (green curves), which are known to have a shorter electron spin flip time, affecting the coherence of the states. For a cooled down system at 55 K (blue curves) and reference of nonchiral 9DT molecules (black curves) the asymmetry is much lower indicating no CISS effect in the devices.

The $I-V$ difference observed under different excitation polarizations, due to the CISS effect, is diminished once higher voltages are applied, at approximately 2 V, as shown in Figure 2b inset for negative bias. This can be explained by the strength of the spin−orbit coupling (SOC) of the charge passing through a chiral monolayer with the chiral potential.[28,29] In the literature, similar response of 0.5 eV was measured for helical chiral double-stranded DNA oligomers.[28] Twice this value is assigned to be the energy gap between two different spin states. Therefore, we can assume that the CISS pseudogap for polyalanine is in the same order of magnitude, around 1 eV.

Measurements of the change in current response with the tuning of the light illumination flux and polarization measured at a constant negative bias voltage of −1.5 V show that the CCW circular polarization had the weakest current response similarly to the previous $I-V$ measurement, while CW circular polarization had the strongest current with the linear polarization in between these two (Figure 2c). The CISS response does not grow linearly with the intensity of the excitation. This can be ascribed to the fact that at high excitation power the Auger process, which does not conserve spin, becomes dominant. As expected, the linear response is somewhat between the CCW and CW circular polarization response. This agrees with the understanding that linear polarization holds equal components of CCW and CW polarizations, thus, creating also an equal amount of opposite spin carriers in the NCs. Therefore, we should expect that the linear response would be the sum of the response of both circular polarizations at half the intensity. However, the linear response is closer to CW response, and the difference may be ascribed to the induced chiral effects by the linkers that change the symmetric response of the NCs to linear polarization. Another effect could be the nonlinearity of the collective spin coherence time T2 decay at different intensities and polarizations.[30]

We measured the absolute response of the device with chiral molecules and 610 nm CdSe NCs, under different illumination wavelengths and polarizations and compared them to a reference sample without NCs. The absolute response for the device is shown in Figure 3a. It was calculated by subtracting the dark current response from the polarized (CW or CCW) response, then by normalizing it with the dark current response. Figure 3a presents the device behavior with above band gap illumination, 532 nm (red curves), and below-the-band gap 660 nm illumination (blue curves). As a reference, we measured a device without the NCs layer on top of the chiral molecules. The device with chiral molecules and NCs, illuminated above band gap has a response 2 orders of magnitude larger than the device with below band gap illumination, and 4 orders of magnitude larger than the device without NCs. Moreover, the fact that the absolute response is dependent on the bias agrees well with the diode-like characteristics of the NCs junction, unlike the reference measurements where the absolute response is constant. From these measurements we presume that the previous $I-V$ measurements can be mainly attributed to charges created in the NCs.

The asymmetry between the circular polarizations normalized to the linear response was calculated for four different devices (Figure 3b). This was done by subtracting the linear current response from the circular polarization responses, then normalizing it by dividing by the linear current response. In this figure we compared the influence of the chirality of the molecules and NCs size on the performance of the devices. For

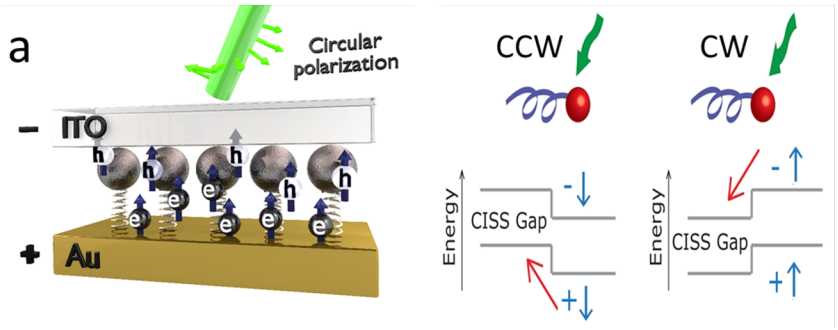

Figure 4. (a) Schematic representation of the charge separation process in the device. Electron−hole pairs are created when exciting with a laser, CW in this example, with spins facing up. As long as the spin state is preserved under negative bias the CISS effect prefers the transfer of the electrons through the chiral monolayer. (b) In a more general energetic perspective, there is a pseudo CISS gap which changes according to the exciton polarization on the NCs. Charges carrying the favored spin, will have energetic preference to transfer through the chiral monolayer.

DOI: 10.1021/acsphotonics.5b00343
ACS Photonics 2015, 2, 1476−1481

the device with chiral molecules and 610 nm CdSe NCs (red curve), a distinct asymmetry is seen between CW and CCW illuminations, especially in the negative bias. This is peculiar since the asymmetry difference is measured in the device in spite of its narrow layer (~4 nm) of the chiral molecules. The difference is much smaller at the positive bias, which agrees with Figure 2b, where the CCW polarization becomes stronger in positive biases, thus, showing spin coherence influence on charge separation. To further study the effect and connect it with the spin coherence time, measurements were performed with a monolayer of smaller CdSe NCs, with the main emission peak at 520 nm, adsorbed on top of the chiral monolayer. The bandgap of the smaller NCs was closer to the excitation laser's wavelength of 532 nm, which would enable better spin coherence since only a narrow-energy ensemble of dots is excited exactly to the bandgap.[21] On the other hand, in previous studies of smaller CdSe NCs (with the absorption peak of 498 and 578 nm), a fast electron spin state flip was measured.[21] Overall, spin coherence T1 times are expected to be shorter with smaller dots. This compromises the charge separation process in our device configuration. The asymmetry measurements for the smaller CdSe NCs, shown in green in Figure 3b, demonstrate a spin-dependent charge separation effect that is weaker than for the larger NCs. Thus, the measurements seem to be sensitive to the spin-coherent time of the dots and to the electron spin flip, which in the case of smaller CdSe NCs becomes more dominant and compromises the charge separation effect.

Smaller charge separation effect could be also predicted due to changes in the excited states lifetime upon cooling. Spin coherence and excited state lifetimes are expected to be 2 orders of magnitude longer at low temperatures.[31−33] However, in the helical chiral molecules it has been shown that below 150 K the chiral molecules used in this study undergo structure and electrical phase transition,[34,35] thus, rendering a weaker chiral-induced state that may shorten dramatically the substrate spin lifetime. Therefore, upon cooling, one would expect an increase of charge separation down to 150 K, with the effect disappearing at lower temperatures. For a cooled down system (blue curves) and reference room temperature measurements of nonchiral 1,9-nonanedithiol (9DT) molecules (black curves), the asymmetry is much lower, indicating negligible charge separation effect in the devices. Indeed, at 55 K, the asymmetry results for the chiral molecules (in blue) are similar for both circular polarizations. All results are weak relative to the room temperature measurements, indicating that the charge separation is less prominent at low temperatures.

In conclusion, we have demonstrated nanoscale charge separation using a thin layer device based on chiral molecules and semiconductor NCs. We have shown that the device was sensitive to the circular polarization excitation of the NCs, measuring a difference in the current responses in our device. Chiral imprinting on NCs by the organic linkers may induce response even for nonpolarized light. The measured difference was attributed to the CISS effect and to room temperature charge separation at the small 4 nm scale. Our measurements were susceptible to the spin state dynamics (electron and hole spin flip times) of the excitons created in the NCs, which are dependent on the size of the NCs used. Similar effects for small scale charge separation are measured in biological photosynthetic systems where the molecules are chiral as well. In the future, devices using the measured effect could be fabricated with nanosized features.

METHODS

The charge separation device was fabricated using upper and lower contacts with adsorbed molecules and NCs in between, as shown in Figure 1a. The 150 nm lower gold contacts were evaporated and pattered, using conventional photolithography methods, on SiO_2 substrate, followed by a dielectric insulation layer of 150 nm Al_2O_3. The device active area was attained by wet etching 40 × 50 μm^2 windows in the Al_2O_3 layer down to the lower contact, followed by a selective adsorption of the chiral, charge separation layer and the CdSe NCs on top of the gold bottom contact. A 4−7 nm thick Al_2O_3 tunnel barrier was evaporated in a cooled chamber on top of the NCs, followed by a top transparent indium tin oxide (ITO) contact. To achieve better statistics, many windows were opened in each device (as shown in Figure 1a). The full device was mounted and wire bonded to a 44 header chip (Figure 1b). A close up of the active area is shown in the inset of Figure 1b.

The adsorbed hybrid (chiral molecule-NCs) layer was realized by chemically connecting the desired NCs to a self-assembled monolayer of molecules on top of the gold contacts. α-Helix L-polyalanine (AHPA-L) molecules (Sigma-Aldrich Co. LLC), diluted to a 1 mM ethanol solution, were used as covalent chiral linkers. 1,9-Nonanedithiol (9DT; Sigma-Aldrich Co. LLC) nonchiral molecules were used for reference measurements. Two types of core CdSe NCs were studied, one with a main emission peak at 610 nm and one at 520 nm (Sigma-Aldrich Co. LLC), with 40 nm distribution widths. The NCs solution was further diluted in toluene solvent to the concentration of 0.5 (mg/mL).

The hybrid layer preparation was performed in three steps. First, the devices were left in absolute ethanol for 20 min, then the devices were incubated in the ethanol solution of the organic molecules; 3 h for chiral molecules or overnight for 9DT molecules. The excess of the organic molecules was removed from the surface by washing the sample with ethanol several times. Lastly, the samples were dried under nitrogen and introduced into a toluene solution containing the NCs for 4 h. The whole process was performed under inert atmosphere. Figure 1c displays a SEM micrograph of the adsorbed CdSe NCs on top of a chiral monolayer.

The NCs were optically excited with a diode-pumped solid-state continuous-wave (DPSS CW) 532 nm (660 nm) laser with typical laser power of 20 mW. The clockwise (CW) or counterclockwise (CCW) circular polarization illumination was achieved using a linear polarizer in the optical path (45° or 315°, accordingly) followed by a quarter wave plate. The ensuing constant laser intensity was monitored using a detector during measurements. A simple mechanical shutter was placed along the optical path to compare light and dark measurements. $I-V$ transport measurements were performed with a Keithley 2400 source meter and a 6485 picoammeter.

Structure of the chiral monolayer on the gold was characterized by Polarization modulation-infrared reflection-adsorption spectroscopy (PM-IRRAS) and atomic force microscopy (AFM) methods.[36,37] The PM-IRRAS spectra is displayed in Figure 1d. The information about the tilt angle of the helix axis from the surface normal can be obtained from the intensity of amide I and amide II bands, which appear at 1663 and 1549 cm^{-1}, respectively[27,38] (see Supplementary PM-IRRAS Measurements). The value of the tilt angle γ of the helix with respect to the surface normal was found to be $\gamma = 46°$. The thickness of the chiral monolayer was characterized by AFM

DOI: 10.1021/acsphotonics.5b00343
ACS Photonics 2015, 2, 1476−1481

(Figure 1e). An area of about 400 nm^2 was removed by scratching the molecules from the surface (see inset). The uncovered area shows a depth of about δ = 3.0 nm relative to the unscratched area. Taking into account both measurements, we observe that the chiral monolayer height is about 4.3 nm.

SUPPLEMENTARY PM-IRRAS MEASUREMENTS

The PM-IRRAS spectra is shown in Figure 2b. The information about the tilt angle of the helix axis from the surface normal can be obtained from the intensity of amide I and II bands, which appear at 1663 and 1549 cm^{-1}, respectively.[27,38]

The orientation of the peptide molecules immobilized on the gold surface was determined using the following equation:[27] $(I_1/I_2) = 1.5 \times ((3\cos^2\gamma - 1)(3\cos^2\theta_1 - 1) + 2/(3\cos^2\gamma - 1)(3\cos^2\theta_2 - 1) + 2)$, where I_1 and I_2 are the absorbance of amide I and II bands, respectively, γ is the tilt angle of the helical axis with respect to the surface normal, and $\theta_{1,2}$ are the angles between the transition moment and the helix axis. The values of θ_1 and θ_2 were set to 39° and 75°, respectively.[27] The value of the tilt angle γ of the helix with respect to the surface normal was found to be γ = 46°.

AUTHOR INFORMATION

Corresponding Author

*E-mail: paltiel@mail.huji.ac.il.

Notes

The authors declare no competing financial interest.

ACKNOWLEDGMENTS

We acknowledge the financial support by the Volkswagen Foundation, the Ministry of Science Technology and Space, 210514, and Yissum, the I.P. Company of the Hebrew University of Jerusalem.

ABBREVIATIONS

CISS, chiral-induced spin selectivity; SAM, self-assembled monolayer; NC, nanocrystals; FET, field effect transistor; CW, clockwise; CCW, counter clockwise; SOC, spin−orbit coupling; 9DT, 1,9-nonanedithiol; ITO, indium tin oxide; AHPA-L, α helix L-polyalanine; DPSS CW, diode-pumped solid-state continuous-wave; PM-IRRAS, Polarization modulation-infrared reflection-adsorption spectroscopy; AFM, atomic force microscopy

REFERENCES

(1) Reed, G. In *Silicon Photonics*; Reed, G. T., Ed.; John Wiley and Sons, Ltd.: Chichester, U.K., 2008.

(2) Shah, a. V.; Platz, R.; Keppner, H. Thin-Film Silicon Solar Cells: A Review and Selected Trends. *Sol. Energy Mater. Sol. Cells* **1995**, *38*, 501−520.

(3) Carlson, R. O. Electrical Properties of Near-Degenerate Boron-Doped Silicon. *Phys. Rev.* **1955**, *100*, 1075−1078.

(4) Nitzan, A.; Ratner, M. a. Electron Transport in Molecular Wire Junctions. *Science* **2003**, *300*, 1384−1389.

(5) Dor, O. B.; Yochelis, S.; Mathew, S. P.; Naaman, R.; Paltiel, Y. A Chiral-Based Magnetic Memory Device without a Permanent Magnet. *Nat. Commun.* **2013**, *4*, 2256.

(6) Göhler, B.; Hamelbeck, V.; Markus, T. Z.; Kettner, M.; Hanne, G. F.; Vager, Z.; Naaman, R.; Zacharias, H. Spin Selectivity in Electron Transmission through Self-Assembled Monolayers of Double-Stranded DNA. *Science* **2011**, *331*, 894−897.

(7) Xie, Z.; Xie, Z.; Markus, T. Z.; Cohen, S. R.; Vager, Z.; Gutierrez, R.; Naaman, R. Spin Specific Electron Conduction through DNA Oligomers. *Nano Lett.* **2011**, *11*, 4652−4655.

(8) Naaman, R.; Waldeck, D. H. Chiral-Induced Spin Selectivity Effect. *J. Phys. Chem. Lett.* **2012**, *3*, 2178−2187.

(9) Yeganeh, S.; Ratner, M. a.; Medina, E.; Mujica, V. Chiral Electron Transport: Scattering through Helical Potentials. *J. Chem. Phys.* **2009**, *131*.01470710.1063/1.3167404

(10) Medina, E.; Lopez, F.; Ratner, M. A.; Mujica, V. Chiral Molecular Films as Electron Polarizers and Polarization Modulators. *Europhys. Lett.* **2012**, *99*, 17006.

(11) Gutierrez, R.; Díaz, E.; Naaman, R.; Cuniberti, G. Spin-Selective Transport through Helical Molecular Systems. *Phys. Rev. B: Condens. Matter Mater. Phys.* **2012**, *85*, 081404.

(12) Gersten, J.; Kaasbjerg, K.; Nitzan, A. Induced Spin Filtering in Electron Transmission through Chiral Molecular Layers Adsorbed on Metals with Strong Spin-Orbit Coupling. *J. Chem. Phys.* **2013**, *139*.11411110.1063/1.4820907

(13) Skourtis, S. S.; Beratan, D. N.; Naaman, R.; Nitzan, A.; Waldeck, D. H. Chiral Control of Electron Transmission through Molecules. *Phys. Rev. Lett.* **2008**, *101*, 238103.

(14) Peng, X.; Manna, L.; Yang, W.; Wickham, J.; Scher, E.; Kadavanich, A.; Alivisatos, A. Shape Control of CdSe Nanocrystals. *Nature* **2000**, *404*, 59−61.

(15) Mocatta, D.; Cohen, G.; Schattner, J.; Millo, O.; Rabani, E.; Banin, U. Heavily Doped Semiconductor Nanocrystal Quantum Dots. *Science* **2011**, *332*, 77−81.

(16) Klimov, V. *Nanocrystal Quantum Dots*; CRC Press: Boca Raton, FL, 2010.

(17) Kim, J.; Wong, C. Y.; Scholes, G. D. Exciton Fine Structure and Spin Relaxation in Semiconductor Colloidal Quantum Dots. *Acc. Chem. Res.* **2009**, *42*, 1037−1046.

(18) Huxter, V. M.; Kim, J.; Lo, S. S.; Lee, A.; Nair, P. S.; Scholes, G. D. Spin Relaxation in Zinc Blende and Wurtzite CdSe Quantum Dots. *Chem. Phys. Lett.* **2010**, *491*, 187−192.

(19) Horodyska, P.; Nemec, P.; Sprinzl, D.; Maly, P.; Gladilin, V. N.; Devreese, J. T. Exciton Spin Dynamics in Spherical CdS Quantum Dots. *Phys. Rev. B: Condens. Matter Mater. Phys.* **2010**, *81*, 24.

(20) Němec, P.; Nahálková, P.; Sprinzl, D.; Malý, P.; Gladilin, V. N.; Devreese, J. T. Spin-Sensitive Differential Transmission Experiments in Quasi-Spherical CdS Quantum Dots. *Phys. Status Solidi C* **2006**, *3*, 4291−4294.

(21) Ma, H.; Jin, Z.; Zhang, Z.; Li, G.; Ma, G. Exciton Spin Relaxation in Colloidal Cdse Quantum Dots at Room Temperature. *J. Phys. Chem. A* **2012**, *116*, 2018−2023.

(22) Koslovsky, O.; Yochelis, S.; Livneh, N.; Harats, M. G.; Rapaport, R.; Paltiel, Y. Simple Method for Surface Selective Adsorption of Semiconductor Nanocrystals with Nanometric Resolution. *J. Nanomater.* **2012**, *2012*, 1−5.

(23) Neubauer, A.; Yochelis, S.; Amit, Y.; Banin, U.; Paltiel, Y. Highly Sensitive Room Temperature Infrared Hybrid Organic-Nanocrystal Detector. *Sens. Actuators, A* **2015**, *229*, 166−171.

(24) Maoz, B. M.; Chaikin, Y.; Tesler, A. B.; Bar Elli, O.; Fan, Z.; Govorov, A. O.; Markovich, G. Amplification of Chiroptical Activity of Chiral Biomolecules by Surface Plasmons. *Nano Lett.* **2013**, *13*, 1203−1209.

(25) Lawton, T. J.; Pushkarev, V.; Wei, D.; Lucci, F. R.; Sholl, D. S.; Gellman, A. J.; Sykes, E. C. H. Long Range Chiral Imprinting of Cu(110) by Tartaric Acid. *J. Phys. Chem. C* **2013**, *117*, 22290−22297.

(26) Govorov, A. O.; Fan, Z.; Hernandez, P.; Slocik, J. M.; Naik, R. R. Theory of Circular Dichroism of Nanomaterials Comprising Chiral Molecules and Nanocrystals: Plasmon Enhancement, Dipole Interactions, and Dielectric Effects. *Nano Lett.* **2010**, *10*, 1374−1382.

(27) Miura, Y.; Kimura, S.; Imanishi, Y.; Umemura, J. Formation of Oriented Helical Peptide Layers on a Gold Surface Due to the Self-Assembling Properties of Peptides. *Langmuir* **1998**, *14*, 6935−6940.

(28) Naaman, R.; Waldeck, D. H. Chiral-Induced Spin Selectivity Effect. *J. Phys. Chem. Lett.* **2012**, *3*, 2178−2187.

(29) Winkler, R. *Spin-Orbit Coupling Effects in Two-Dimensional Electron and Hole Systems*, Issue 191; Springer Science and Business Media: Berlin; Heidelberg, 2003.

DOI: 10.1021/acsphotonics.5b00343
ACS Photonics 2015, 2, 1476−1481

(30) Uskov, a. V.; Boucher, Y.; Le Bihan, J.; McInerney, J. Theory of a Self-Assembled Quantum-Dot Semiconductor Laser with Auger Carrier Capture: Quantum Efficiency and Nonlinear Gain. *Appl. Phys. Lett.* **1998**, *73*, 1499−1501.
(31) Donegá, C. D. M.; Bode, M.; Meijerink, A. Size- and Temperature-Dependence of Exciton Lifetimes in CdSe Quantum Dots. *Phys. Rev. B: Condens. Matter Mater. Phys.* **2006**, *74*, 1−9.
(32) Syperek, M.; Yakovlev, D.; Yugova, I.; Misiewicz, J.; Sedova, I.; Sorokin, S.; Toropov, a.; Ivanov, S.; Bayer, M. Long-Lived Electron Spin Coherence in CdSe/Zn(S,Se) Self-Assembled Quantum Dots. *Phys. Rev. B: Condens. Matter Mater. Phys.* **2011**, *84*, 1−8.
(33) Zhang, Z.; Jin, Z.; Ma, H.; Xu, Y.; Lin, X.; Ma, G.; Sun, X. Room-Temperature Spin Coherence in Zinc Blende CdSe Quantum Dots Studied by Time-Resolved Faraday Ellipticity. *Phys. E* **2014**, *56*, 85−89.
(34) Carmeli, I.; Kumar, K. S.; Heifler, O.; Carmeli, C.; Naaman, R. Spin Selectivity in Electron Transfer in Photosystem I. *Angew. Chem.* **2014**, *126*, 9099−9104.
(35) Dor, O. B.; Morali, N.; Yochelis, S.; Baczewski, L. T.; Paltiel, Y. Local Light-Induced Magnetization Using Nanodots and Chiral Molecules. *Nano Lett.* **2014**, *14*, 6042−6049.
(36) López-Pérez, D. E.; Revilla-López, G.; Jacquemin, D.; Zanuy, D.; Palys, B.; Sek, S.; Alemán, C. Intermolecular Interactions in Electron Transfer through Stretched Helical Peptides. *Phys. Chem. Chem. Phys.* **2012**, *14*, 10332−10344.
(37) Naaman, R.; Vager, Z. Spin Selective Electron Transmission through Monolayers of Chiral Molecules. *Top. Curr. Chem.* **2010**, *298*, 237−257.
(38) Kennedy, D. F.; Crisma, M.; Toniolo, C.; Chapman, D. Studies of Peptides Forming 310- and.alpha.-Helixes and.beta.-Bend Ribbon Structures in Organic Solution and in Model Biomembranes by Fourier Transform Infrared Spectroscopy. *Biochemistry* **1991**, *30*, 6541−6548.

DOI: 10.1021/acsphotonics.5b00343
ACS Photonics 2015, 2, 1476−1481